DEUTSCHES ELEKTRONEN-SYNCHROTRON

a 1 9 9 6 0 0 1 a

Photons and Pomerons in Photoproduction at HERA

U. Mallik

Phys. and Astronom. Dept., Univ. of Iowa, Iowa City, USA

NOTKESTRASSE 85   -   22607 HAMBURG

To be sure that your preprints are promptly included in the
HIGH ENERGY PHYSICS INDEX,
send them to (if possible by air mail):

DESY	DESY-IfH
Bibliothek	Bibliothek
Notkestraße 85	Platanenallee 6
22607 Hamburg	15738 Zeuthen
Germany	Germany

Photons and Pomerons in Photoproduction at HERA

Usha Mallik
The University of Iowa
(representing H1 and ZEUS collaborations)

Abstract

The physics of transition between non-perturbative and perturbative QCD at low x has been explored at the ep collider HERA. Some recent results from the H1 and ZEUS experiments are discussed.

1 Introduction

Deep Inelastic Scattering (DIS) has been one of the most resourceful ways to examine the internal structure of hadrons. Leptons, structureless compared to hadrons, are used as probes. The experiments are difficult and time consuming, as seen from the experiences of SLAC, EMC, BCDMS, E665, CDHS, CCFR[1] etc. All these are fixed target experiments with electron[2], muon[3], and neutrino beams[4], performed in the kinematic ranges shown in Fig.1 (a). HERA, the first ep collider, covers a very large unexplored kinematic domain. It can extend to the fixed target region by varying either the lepton or the proton beam energy in order to establish continuity with the fixed target experimental results. Since electrons interact with charged particles predominantly through photon exchange, HERA also provides an opportunity to study the characteristics of photons from quasi-real to virtual.

The low x region ($10^{-4} \sim 10^{-5}$) at moderate Q^2 is a newly explored kinematic regime where perturbative calculations of Quantum ChromoDynamics (QCD) are expected to work. This is also a region where scaling violation is large and the sea density is high where the transition from non-perturbative to perturbative QCD (pQCD) is expected to take place. New phenomena

observed in this transition region might be calculated with the help of pQCD. In other words, theoretical calculations can be tested under new and novel experimental situations in this region. At HERA, we operationally describe processes up to a virtuality of $Q^2 \leq 4\,\mathrm{GeV}^2$ as photoproduction; the reason is explained later. Since HERA covers the kinematic region where photon propagators range from quasi-real ($Q^2 \simeq 0$) to virtual (DIS), the changing nature of the photon can be critically studied. Photoproduction results have historically been explained by a combination of the Vector Dominance Model (VDM)[7] and Regge phenomenology[9], i.e., non-perturbative theory. The DIS region, on the other hand, has been described by pQCD. A challenge for HERA is to study and understand the change or the transition region between the non-perturbative and the perturbative domain. In many cases the same interaction is studied with variation of parameters and the results then compared with pQCD predictions. The hope is to understand which of these, if any, parameters sets the appropriate scale for QCD. We denote the non-perturbative domain as the 'old' domain and the transition region as the 'new' domain. This 'new' or the transition domain is critically studied both in photoproduction, i.e., interactions with $Q^2 \leq 4$ GeV^2 and in DIS interactions as well. In this talk I describe the HERA photoproduction results; the next speaker will discuss the DIS results. We start
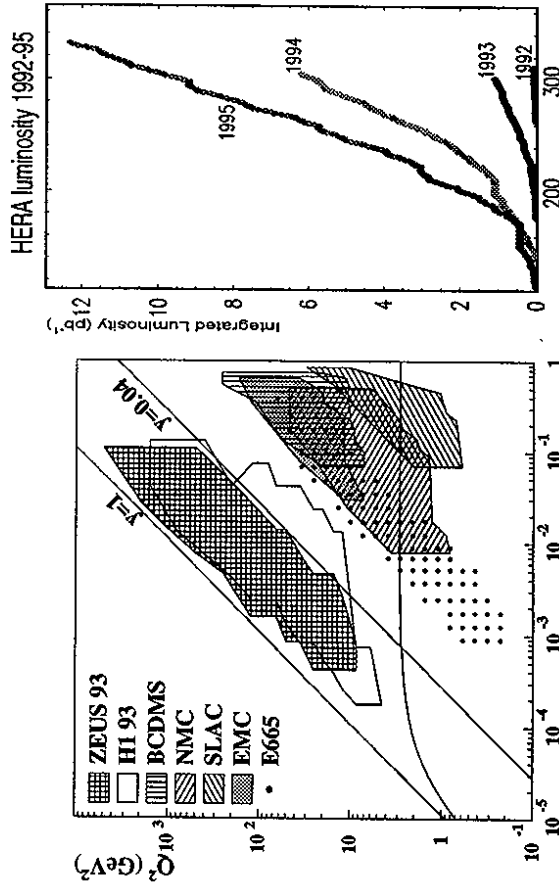
Figure 1: (a) A comparison of the kinematic reach of HERA with the fixed target DIS experiments; (b) The luminosity delivered by HERA to date.

with the photoproduction reactions which were understood with VDM and Regge phenomenology[8, 9]; these are measured at HERA and compared

The two detectors are similar, both are multipurpose and magnetic, but complementary to each other in specific details. Both detectors display a forward backward asymmetry to accomodate the forward motion of the c.m. in the lab frame. Both detectors use a right handed coordinate system with the origin(0,0,0) as the Interaction Point (IP). The Z-axis is positive in the forward direction where the polar angle θ is zero. The negative Z direction corresponds to a θ value of 180°.

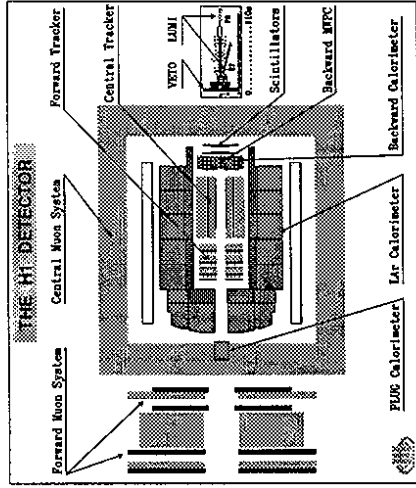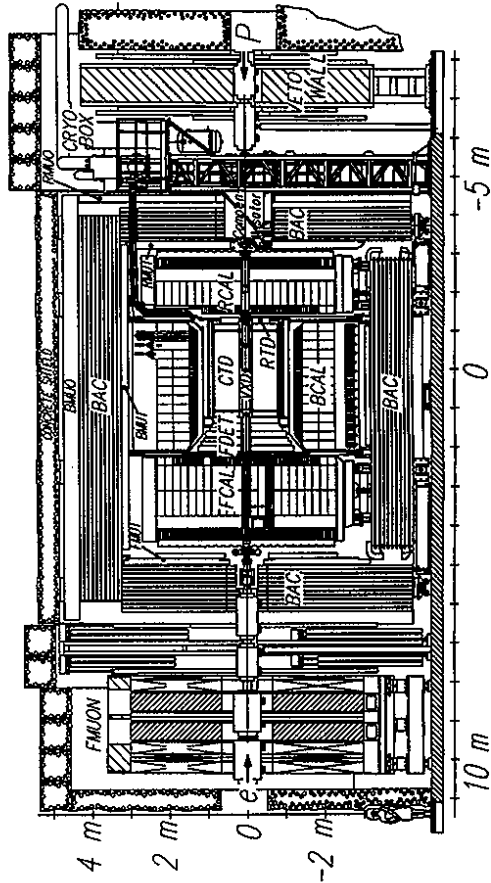THE H1 DETECTOR

Forward Muon System • Central Muon System • Forward Tracker • Central Tracker • VETO LUMI • Scintillators • Backward MPC • Backward Calorimeter

PLUG Calorimeter • LAr Calorimeter

Figure 2: Axial view of the a) H1 and b) ZEUS detector.

Overview of the ZEUS Detector (longitudinal cut)

with the non-perturbative and perturbative models. These measurements are repeated as each parameter (e.g., Q^2, p_t) is varied and the results tested with various predictions. Both light and heavy quark vector mesons productions are discussed. Comparisons between photon induced reactions at HERA and hadron induced reactions from hadron colliders are made, when photoproduction events of different virtuality are compared with the hadron collider results; the difference and the similarities between the two are noted. Evidence of partonic structure and the structure function of the photon are described. Finally, the structure and the contents of pomerons are discussed.

1.1 HERA, H1 and ZEUS

The HERA collider is located in Hamburg, Germany, at the DESY laboratory. The center-of-momentum (c.m.) energy of HERA is 300 GeV, with the ability to run either polarized electrons or positrons to collide with the proton beam. Figure 1(b) shows the luminosity delivered by HERA to date. While the increase is impressive, the goal of 170 pb^{-1} a year, necessary to critically test the Standard Model, remains for the future with the HERA upgrade. The parameters are noted in Table 1. The two colliding beam experiments, H1 and ZEUS occupy the North and the South intersection regions (IR), respectively. The East IR is being used by HERMES, a polarization experiment which uses the polarized lepton beam impinging on a polarized gas jet target. Hermes has started data taking in 1995. Longitudinal polarizations of higher than 60% have routinely been achieved with the help of spin rotators (which convert the naturally acquired transverse polarization of the beam to longitudinal polarization) at the East IR. The West IR is scheduled for HERA B, a high luminosity CP violation experiment using an internal target in the proton beam. They expect to collect data starting from 1997.

Figure 2 shows the H1 and the ZEUS detectors; the lepton beam approaches the IR from the left and exits through the beam pipe to the right. The outgoing proton/lepton direction is noted as the Forward/Rear direction and the respective detector components are noted with the prefix F/R (ZEUS). Detailed descriptions of H1[5] and ZEUS[6] are given elsewhere.

Table 1: HERA parameters

Parameters	electron Design/Achieved	proton Design/Achieved
nominal energy(GeV)	30/27.5	820
energy range (GeV)	10 - 33	300 - 820
beam current (mA)	58/30	163/50
c.m. energy (GeV)	314/300	
circumference (m)	6336	
no. of coll. bunches	200	
bunch crossing time(ns)	96	

4.

1.2 Kinematics

The kinematics are illustrated in Fig.3 and are described below. Here:

k/k' = four-momentum of the incoming/outgoing e;
p/p' = four-momentum of the incoming/outgoing p;
$s = (p + k)^2$ = square of c.m. energy;
$q = k - k'$ = four-momentum of the virtual photon;
$Q^2 = -q^2$;
$y = \frac{2p \cdot q}{2p \cdot k}$;
$x = \frac{Q^2}{2p \cdot q}$;
$W_{\gamma p}^2 = (q + p)^2$; $W_{\gamma p}$ = photon-proton cm energy;
$t = (p - p')^2$;
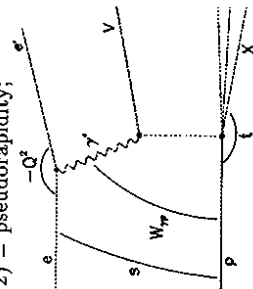$\eta = -ln(tan\theta/2)$ = pseudorapidity;

Figure 3: Diagram of ep collision where a neutral vector meson is produced.

The ZEUS detector covers the pseudorapidity region from $\eta \simeq -3.8$, $\theta \simeq 176°$ in the rear direction to $\eta = 4.3$, $\theta \simeq 2.5°$ in the forward direction. H1 coverage is similar. (The photon fragmentation region, in the rear direction, generally is characterized by $\sim -3.8 \leq \eta \leq -0.75$; similarly, the proton fragmentation region in the forward direction and the central region are characterized, typically, by $\sim 1.1 \leq \eta \leq 4.3$, and $-1.0 \leq \eta \leq 1.0$, respectively.) The scaling variables x and y are related by $Q^2 = xys \simeq 4xyE_eE_p$, where E_e and E_p are the energies of the incoming e and p, respectively.

2 Photoproduction

As mentioned before, we operationally discuss processes as photoproduction up to a virtuality of $Q^2 \leq 4\text{GeV}^2$, beyond which the scattered electron gets detected in the main calorimeter. We define the photon wavefunction to consist of two parts, i.e., $\gamma = \gamma_{direct} + \gamma_{resolved}$, where the direct part represents the pointlike bare photon; photon structure containing partons or virtual mesons as in the VDM is included in the resolved component. Figure 4 shows diagrams in which the photon interacts as a point particle (direct) and in which the photon interacts as a composite, i.e., a parton from the photon interacts with a parton from the proton and the remnants of both the photon and the proton (resolved) are observed. In the direct photon picture the entire photon partakes in the interaction; so the momentum fraction of the photon measured from the detected particles from the interaction, $x_\gamma \simeq 1$. In the resolved interaction, part of the photon momentum is carried

away by its remnant, hence, the momentum carried by the partons in the central collision provide $x_\gamma < 1$. The photon remnant typically is observed in the rear part of the detector.
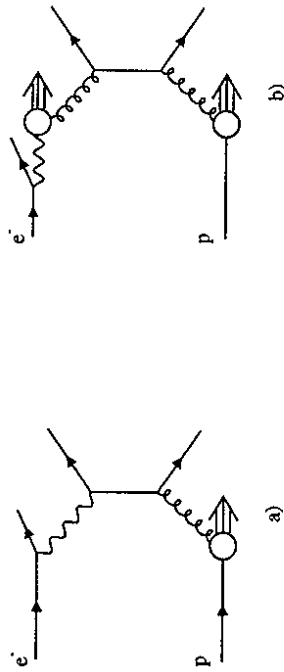

Figure 4: Leading order diagrams of direct and resolved photon interactions.

One hopes that a systematic comparison of experimental results under varying parameters with theoretical calculations will lead to the understanding of the scale to allow pQCD calculations. Various kinematic signatures in an interaction can set such a scale. An interaction where high mass vector mesons are produced using quasi-real photons (e.g. photoproduction of J/ψ), or light quark vector meson production at high virtuality or at high p_t^2, where p_t is the transverse momentum of the detected system (e.g. jets in hard photoproduction) can be used to test the validity of the pQCD models. We explore each of these interactions starting with the 'old' topics, i.e., the validity of the well known VDM models in the framework of Regge theory in photoproduction.

2.1 Total γp cross section

Early experiments showed that quasi-real photons behave much like hadrons: the total photoproduction cross section, $\sigma(\gamma p)$, was shown to be related to the total $\pi^- p$ and $\pi^+ p$ cross section through VDM-inspired relations[8]. The equivalent photon flux, obtained from the Weizacker-Williams formula[10] decreases logarithmically as the virtuality increases; hence the largest contribution to the photoproduction cross section is made by almost real photons. Prior to HERA, the only $\sigma(\gamma p)$ measurements were available for c.m. energy $W_{\gamma p} \leq 20$ GeV, with laboratory photon beam energies up to 100 GeV[11]. The ZEUS and H1 measurements, shown in Fig. 4a, achieve $150 \leq W_{\gamma p} \leq 200$ GeV, corresponding to a laboratory photon beam energy above 5 TeV in a fixed target experiment. Earlier data were parameterized using the Regge model prescription of the total cross section[12] given by $\sigma(\gamma p) = Xs^\epsilon + Ys^{-\eta}$, where X, Y, ϵ and η are constants determined from the data with $\epsilon = 0.0808$ and $\eta = 0.4525$. The first term accounted for the slow rise of the cross section at high energies by incorporating the Regge idea of pomeron exchange and the second term denoted the contribution from all other meson exchanges. A pomeron, in the Regge

photoproduction, exclusive (or elastic) vector meson production calculated in pQCD requires exchange of an object with the quantum numbers of the pomeron. This is alluded to as a 'hard' pomeron.

At H1 and ZEUS experiments, the ρ, ω and the ϕ signals are observed in $\pi^+\pi^-$, $\pi^+\pi^-\pi^0$, and K^+K^- decay modes, respectively[19, 18, 20]. Figure 6 (a) shows a compilation of the elastic ρ photoproduction cross sections with measurements from both H1 and ZEUS. The ρ^0 polarization measured from its decay angular distribution was observed to be transverse. This is in accordance with the expected polarization of the quasi-real photons producing the ρ's, assuming s channel helicity conservation (SCHC).

The $W_{\gamma p}$ dependence of the cross sections is shown for all available exclusive vector meson final states in Fig.7 (a). The data for ρ, ω and ϕ agree well with the soft pomeron picture. The measured cross section ratios are in good agreement with the VDM predictions within the quoted uncertainties[3]

The t dependence of the ρ^0 cross sections was fit to the form $d\sigma/dt = A \cdot exp(-b|t'|)$, with $t' = t - t_{min}$. A compilation of the measurements of the slope parameter b is shown in Fig.6 b). For the 1994 ZEUS data, the scattered p was detected in the Leading Proton Spectrometer (LPS)[21], and thus t' was directly measured in the range $0.07 \leq |t'| \leq 0.4 \mathrm{GeV}^2$. For ω and ϕ, the differential cross sections were measured for the $|t'|$ ranges of $0 \leq |t'| \leq 0.6$ and $0.1 \leq |t'| \leq 0.5$, respectively. The results are summarized in Table 2.

model, is a hypothetical particle with the quantum numbers of vacuum. The so-called Regge trajectories are represented by $\alpha(t) = \alpha(0) + \alpha' t$; for a pomeron $\alpha(0) = 1 + \epsilon = 1.0808$ denotes the intercept on the t-axis, and $\alpha' = 0.25 \mathrm{GeV}^{-2}$ denotes the slope of the trajectory. A fit to recent high energy total cross section measurements in $p\bar{p}$[13] prefers $\alpha(0) \simeq 1.11$. This value is also incorporated into the prediction shown in Fig.5 along with the
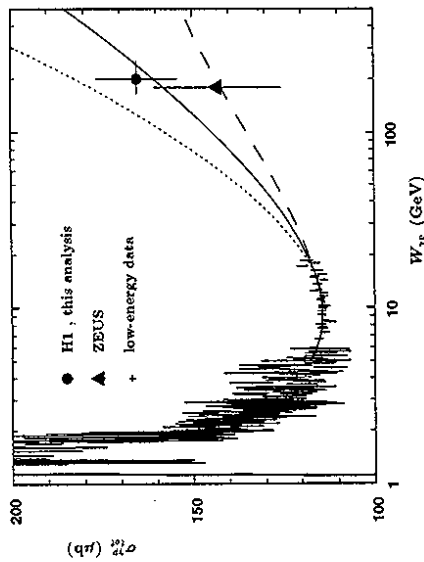

Figure 5: Total photoproduction cross sections. The solid line is the prediction of the DL[14] combined fit of the hadron and low energy photoproduction data and the dashed line is the ALLM[15] parameterization. The dotted line presents the DL parameterization obtained after the recent measurement[13] from CDF.

data at low and high energies[1]. and some of the parameterizations[14, 15]. In the low Q^2 domain, where the non-perturbative approach seems adequate, the pomeron is thought of as 'soft'. Hence the 'soft pomeron' approach seems to still suffice in explaining the total photoproduction cross section at even the very high HERA energies.

2.2 Vector Meson Production: light quark sector

The VDM models originated before any of the photoproduction measurements of ρ, ω, and ϕ. According to VDM, the photon fluctuates into a vector meson (ρ, ω, and ϕ); in elastic photoproduction the vector meson materializes by exchange of the pomeron between the γ and the proton. The soft pomeron is characterized by a weak dependence of the cross section on $\gamma^* p$ c.m. energy, $\sigma_{(\gamma p - v p)} \simeq W_{\gamma p}^{0.22}$, similar to that of the total photoproduction cross section described above. In analogy to the soft pomeron in 'old'

---

[1] In the results, the first uncertainty quoted is statistical and the second is systematic. In the figure the error bars indicate the uncertainties. The inner error bars indicate statistical errors, the outer error bars show the systematic uncertainty (excluding the correlated uncertainty) added in quadrature

[2] γ^* refers to an off-shell photon

Table 2: Elastic photoproduction of light quark vector mesons

Reaction	H1	ZEUS
$\gamma p \to \rho^0 p$		
$<W_{\gamma p}>$ (GeV)	55	70
$\sigma(\gamma p \to \rho^0 p)$ (μb)	$9.1 \pm 0.9 \pm 2.5$	$14.7 \pm 0.4 \pm 2.4$
b (GeV^{-2})	$10.9 \pm 2.4 \pm 1.1$	$9.9 \pm 1.2 \pm 1.4$
r_{00}^{04}	$-0.11 \pm 0.11 \pm 0.04$	$0.055 \pm 0.028 (stat.)$
$\gamma p \to \phi p$		
$<W_{\gamma p}>$ (GeV)		70
$\sigma(\gamma p \to \phi p)$ (μb)		$0.96 \pm 0.19^{+0.21}_{-0.18}$
b (GeV^{-2})		$7.3 \pm 1.0 \pm 0.8$
r_{00}^{04}		$0.03 \pm 0.05 (stat.)$
$\gamma p \to \omega p$		
$<W_{\gamma p}>$ (GeV)		80
$\sigma(\gamma p \to \omega p)$ (μb)		$1.2 \pm 0.1 \pm 0.3$
b (GeV^{-2})		$9.3 \pm 1.7 \pm 1.3$
r_{00}^{04}		$0.07 \pm 0.07 (stat.)$

---

[3] The ϕ total cross section was determined from extrapolating the differential cross section $d\sigma/dt$ to the forward direction $t = t_{min}$ and then integrating the spectrum.
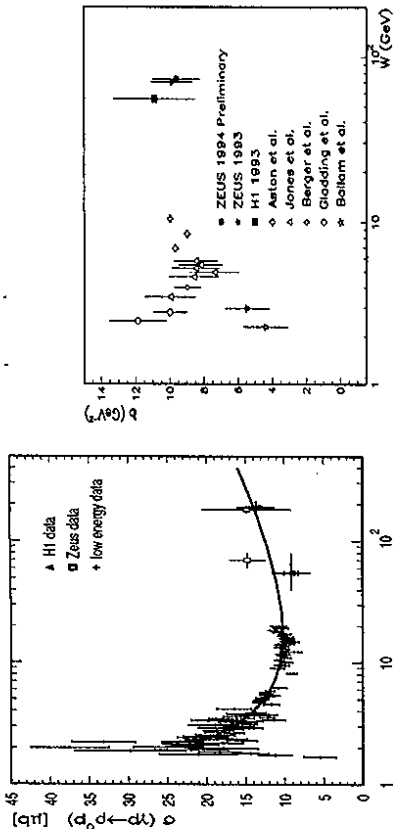
Figure 6: (a) Compilation of elastic ρ photoproduction cross sections. The solid line is the soft pomeron parameterization by Schuler and Sjöstrand[16]. (b) Compilation of b from $d\sigma/dt = A \cdot exp(-b|t'|)$ measurements.

2.3 Heavy quark sector: Charm Production

Elastic J/ψ Production: Elastic photoproduction of J/ψ has been observed[22] with fixed target experiments, but the dependence of the cross section on $W_{\gamma p}$ was not established because of the limited phase space available at the fixed target energies relative to the J/ψ mass ($M_{J/\psi}^2$). HERA experiments measured the elastic photoproduction cross section[25, 26] in the range 40 GeV$\leq W_{\gamma p}$ 180 GeV, clearly establishing the energy dependence shown in Fig. 7 (a). The J/ψ was detected in both leptonic decay modes e^+e^- and $\mu^+\mu^-$.

Perturbative calculations[23, 24] of this diffractive process were thought to be valid in J/ψ production because of the high charm quark mass. Accordingly, the cross section should depend on the square of the gluon momentum density, and the contributing gluon x range in the proton ($x \sim 1/W_{\gamma p}^2$[23], i.e., typically $10^{-3} \sim 10^{-4}$). The lower half of Fig. 7 shows the predictions using three popular parameterizations of the gluon momentum density as input to Ryskin's QCD model[23]. The observed fast rise of this cross section with $W_{\gamma p}$ is thought to arise from the increase in gluon momentum density as x decreases, and is not in agreement with the soft pomeron prediction[17].

The helicity of the J/ψ's is determined from the J/ψ decay angular distribution. The $\cos\theta$ distribution[4] from e^+e^- and $\mu^+\mu^-$ decay modes of the J/ψ in the helicity frame, displayed in Fig 7 (b), shows the J/ψ's polarizations as primarily transverse.

Inelastic J/ψ and Charmed Meson Production: The photon-gluon fusion diagram, an inclusive process, (Fig. 4) is thought to be the primary source of inelastic charm production, as opposed to the elastic or exclusive production of J/ψ which is diffractive. Background processes are expected from the resolved photon process as well as the double diffractive process (with a pomeron exchange) where the proton diffractively dissociates.

---

[4]the $\cos\theta$ distribution is fit to $[1+r_{00}^{04}+(1-3r_{00}^{04})\cos^2\theta)]$ according to a prescription[38], where $r_{00}^{04}=0$ means transverse and 1 means longitudinal polarizations, respectively.
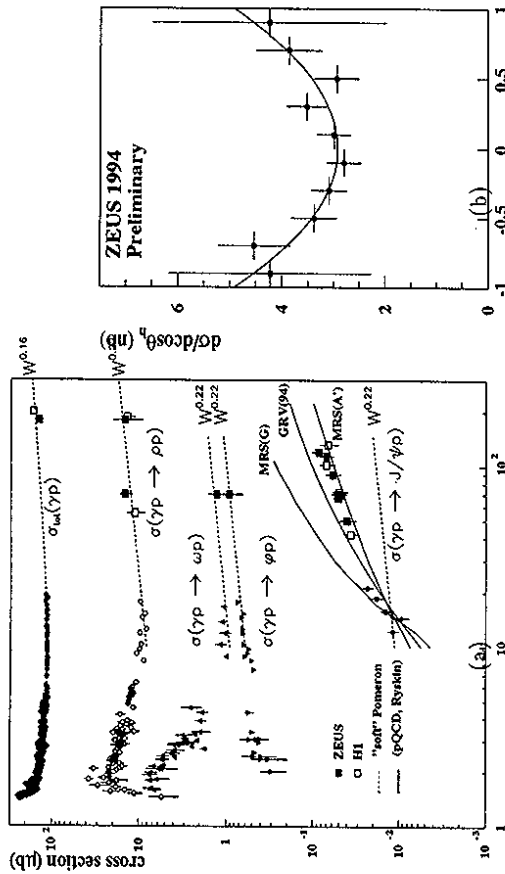

Figure 7: (a) Cross sections of elastic photoproduction of vector mesons. The dotted lines are for the vector meson photoproduction are the DL predictions[17] for a soft pomeron exchange. The J/ψ cross section is described by Rykin's pQCD model[23] using the structure functions shown. (b) decay angular distribution of the J/ψ's in the helicity frame.
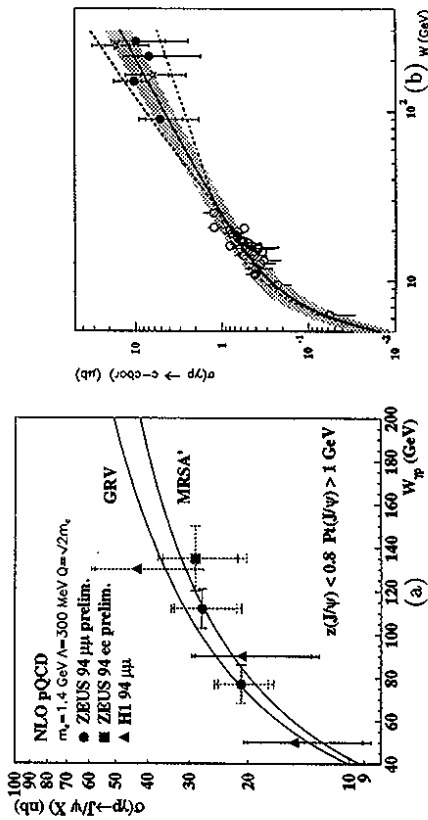

Figure 8: (a) Inelastic photoproduction of J/ψ; The curves represent NLO calculations with proton structure functions as marked. (b) Inelastic photoproduction of D^*'s; the curves represent NLO calculations with various proton and photon structure functions.

Several calculations of J/ψ production[27] and charmed meson production[28] through the photon-gluon fusion process in next-to-leading-order (NLO) of pQCD are available. However, theoretical uncertainties abound. These arise

from the parameterizations of the photon and the proton structure functions, the scale of α_s, the value of the charm mass, etc.

The ZEUS and H1 experiments both observed J/ψ signals in the leptonic decay modes[26]. The D^*, D_s and Λ_c signals were also observed by ZEUS and D^* by H1; the D^* signals were observed from $D^{*+} \to D^0 + \pi^+$ charged conjugate decays[29]. Qualitative agreement between experimental data and theoretical predictions were observed as shown in Fig. 8 (a) and (b). The typical x of the proton probed in these reactions is 10^{-3} and the proton structure functions[5] use a gluon momentum density that increases at low x. The rise in the J/ψ cross section is in agreement with the rise in the gluon density[51, 52] seen in measurements by ZEUS and H1 and will be described by the next speaker.

2.4 Exclusive Vector Meson Production at high virtuality

Exclusive production of ρ^0, ϕ and J/ψ in ep DIS interactions have been observed at HERA, with the scattered electron detected in the calorimeter ($Q^2 \geq 4$ GeV^2). Predictions using pQCD[23, 30, 24, 31] are available for these reactions. The 1993 ZEUS results[32] and the 1994 H1 results[33] for ρ production are displayed in Fig. 9 (a) and (b) (with the elastic photoproduction cross section also shown for comparison). Here the electroproduction cross section has been converted into a virtual photon proton (γ^*p) cross section. The NMC values at lower energies compared to the HERA values indicate a rapid rise of cross section with $W_{\gamma p}$ compared to that in the photoproduction cross section. Presumably, this illustrates a difference between the soft and the hard pomeron exchange. The results have been compared with a theoretical model[30] which applies pQCD calculation based on a similar gluon ladder exchange as that of Ryskin[23]. The model uses longitudinally polarized photons only[30]. The study of the angular distribution[38] of the ρ in the ZEUS data yields $\sim 60\%$ longitudinal polarization at a Q^2 of ~ 9 and 17 GeV^2. Assuming SCHC, 40% of the photon polarization is still transverse. For the H1 data, the longitudinal fraction is observed to be 70%. The data points in the Q^2 and the $W_{\gamma p}$ ranges for the H1 and the ZEUS experiments are noted in Table 3. The Q^2 dependence of the cross section, described by Q^{2n} is shown in Fig. 9(b); the n value determined from the data is also listed in Table 3. (For soft pomeron exchange the cross section falls as Q^4, the pQCD model[30] predicts a faster fall off.)

The DIS ϕ and J/ψ productions, observed by both H1[33] and ZEUS[34], are also listed in Table 3. The longitudinal polarization of the ϕ's observed by ZEUS and H1 (prelim) are, respectively, $0.6\pm0.1^{+0.2}_{-0.1}$ and $0.77\pm0.11\pm0.02$, at the Q^2 and $W_{\gamma p}$ shown in Table 3.

---

[5]Most recent parametrizations of the proton structure function used here are, MRSG (MRS: Martin-Robert-Sterling), MRSA'[48], CTEQ[49] and GRV[50] (GRV: Glück-Reya-Vogt). They all obey the Gribov-Dokshitzer-Lipatov-Altarelli-Parisi (GDLAP) evolution equations[46]. The GRV prescription starts with initial hard parton distribution at 0.3 GeV^{-2} and propagate it according to GDLAP evolution in NLO. In others the gluon momentum density rises as $x^{-\lambda}$ at low x.

Table 3: Exclusive vector meson production in DIS.

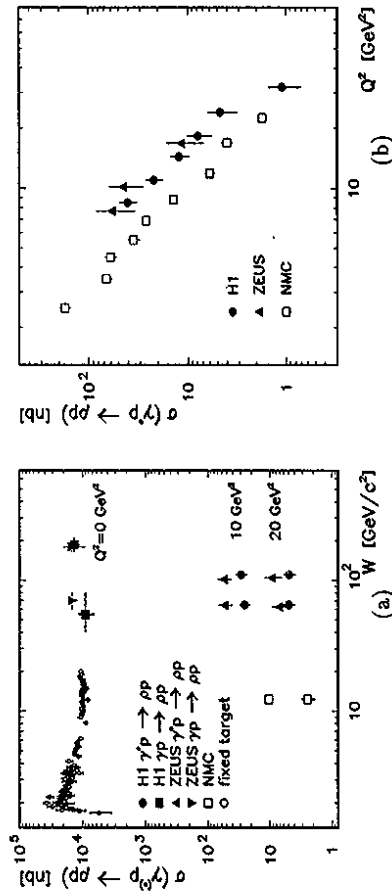| Reaction	H1		ZEUS	
$\gamma^*p \to \rho^0 p$				
$\langle Q^2\rangle$(GeV^2)	≃ 10	≃ 20	≃ 9	≃ 17
$W_{\gamma p}$(GeV)	≃ 65	≃ 115	≃ 62	≃ 100
(Q^{2n}) : n value	2.5 ± 0.5 ± 0.2		2.1 ± 0.4$^{+0.7}_{-0.3}$	
	prelim.			
$\gamma^*p \to \phi p$				
$\langle Q^2\rangle$(GeV^2)	8.3	14.8	8.2	14.7
$(W_{\gamma p})$(GeV)	95	100	94	99
$\sigma(\gamma^*p \to \phi p)$(nb)	~10	~3	10.2 ± 2.2	3.1 ± 0.7
(Q^{2n}) : n value	2.0 ± 0.6		2.1 ± 0.6	
$\gamma^*p \to J/\psi p$			prelim	
$\langle Q^2\rangle$(GeV^2)	10	20	7	
$(W_{\gamma p})$(GeV)	88	88	25	
$\sigma(\gamma^*p \to J/\psi p)$(nb)	17 ± 6.3	6.6 ± 1.6	8.0$^{+5.2}_{-2.0}$	
(Q^{2n}) : n value	2.0 ± 0.6		2.1 ± 0.6	

(a)

(b)

Figure 9: (a) Cross section of exclusive ρ production in $\gamma^*p \to \rho p$ vs $W_{\gamma p}$ (at $Q^2 \sim 10$ and 20 GeV^2). The rise in cross section with $W_{\gamma p}$ observed in DIS is faster than that at $Q^2 \simeq 0$. (b) Cross section for exclusive ρ production in $\gamma^*p \to \rho p$ as a function of Q^2.

2.5 Photoproduction at High Transverse Momentum.

Vector mesons e.g., ρ^0 and ϕ productions with $p_t^2 > 1.0$ GeV^2 have been observed; detailed studies have begun. Preliminary indications are that the diffractive dissociation process dominates.

Dijet Production in Direct and Resolved Photon Interactions:
In hard photoproduction, i.e., in events with high p_t, jet measurements are compared with pQCD predictions in an attempt to understand whether the measurements agree with the predictions, and if so, in which kinematic region is the agreement observed. Events with two jets with a minimum p_t of 7 GeV and with reasonable p_t balance are selected. The details of the jet algorithm, event selection and Monte Carlo are described elsewhere[35, 36]. The direct and the resolved photoproduction events are distinguished by the values of x_γ obtained from the observed jets. The pQCD calculations are made in leading order (LO)[35]; the measurements and the theoretical predictions are shown in Fig. 10. Direct photon events are selected by $x_\gamma \geq 0.75$; the agreement between the data and the theoretical models is at best within ~ 20% for direct photon events (with the choice of the 'best' photon structure function). The resolved photon events agree with the predictions only in shape. Studies are continuing in order to better understand the various parameters, scales, cut-offs, jet algorithms and the use of Monte Carlos.

2.6 Photons as Hadrons

Comparison of Photon and Hadron induced Reactions: Quasi-real photons, known to behave like hadrons[8] in interactions, have been described in VDM models. The H1 experiment extended the comparison of various kinematic quantities and events shapes between photons of different virtualities in the photon induced reactions with similar quantities in hadronic reactions[39]. In the photon fragmentation region, here $-3 \leq \eta \leq -2$, the photons clearly show a rise in p_t^2 per unit rapidity as a function of Q^2. This is shown in Fig. 11 (a). However, the virtuality seems to have

Figure 11: (a) Normalized transverse energy E_T flow in the hadronic c.m. vs η^* at various values of Q^2. (b) E_T distribution per unit of η^* in the central region ($-0.5 < \eta^* < 0.5$) and in the photon fragmentation region ($-3 < \eta^* < -2$). Two different MC models are shown, the lower(upper) curves correspond to the central (photon fragmentation) region.

little effect in the central region[6], here $-0.5 \leq \eta \leq 0.5$ (Fig.11 (b)). Figure

---

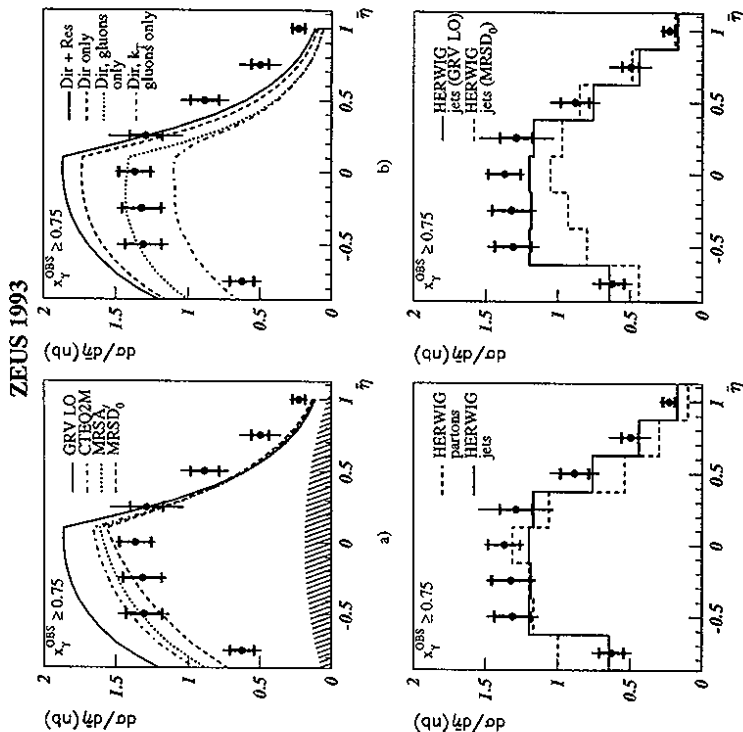[6]The MC, however, does not describe the data very well.

Figure 10: The solid circles are corrected ZEUS data. The shaded band shows the correlated uncertainty from measurement of energy in the calorimeter and the integrated luminosity. ($\bar{\eta}$ is the average η of the dijets). In a) the data are compared to LO QCD calculations using several parton distribution sets for the proton and the GS2[37] set for the photon. In b) the data are compared to the LO QCD calculation of a) using the GRV LO parton distribution set for the proton, the same calculation but omitting the resolved contribution with $x_\gamma \geq 0.75$, including only gluon induced direct photon processes and the 'k_T factorized' curve. In c) the data are compared to HERWIG Monte Carlo estimates of the cross section using partons and final state jets. For these HERWIG histograms we have used the GRV LO (LAC1) proton (photon) parton distribution set. In d) the data are compared to HERWIG jet cross sections using the GRV (LAC1) and MRSD0 (LAC1) proton (photon) parton distribution sets.
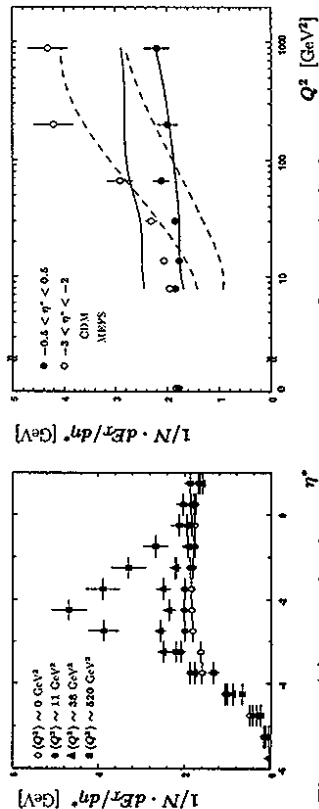
12 shows a comparison of the H1 results in the central region with those from the hadron colliders ordered according to the c.m. energies. It is clear
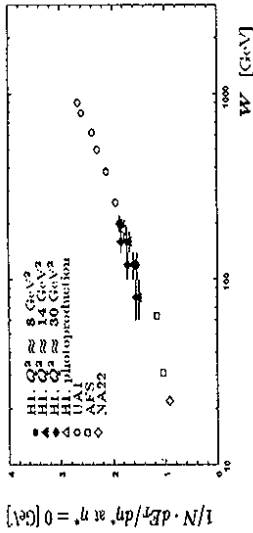
Figure 12: Normalized transverse energy E_T in the central region as a function of the hadronic c.m. energy. The HERA data at various Q^2 are compared with data from hadron-hadron collisions ($p\bar{p}$: UA1, pp: NA22 and AFS). Systematic errors are not shown.

that the hadron and the photon induced reactions look alike in the central region independent of Q^2. Not only does the transverse energy distribution not seem to depend on Q^2, but also the event distributions according to the maximum event rapidity, η_{max}, (i.e., the event shapes) between the hadron and the photon induced reactions look alike, independent of the c.m. energy, as observed from the distributions shown in Fig. 13 (a) and (b). Hence
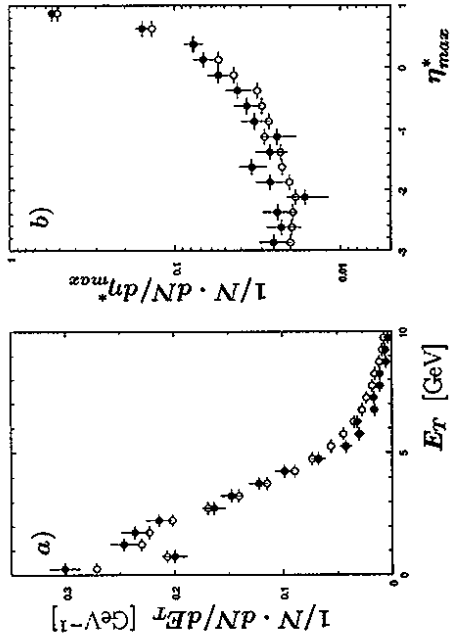
Figure 13: (a) Uncorrected E_T distribution in the central region ($-0.5 < \eta^* < 0.5$) per unit of η^*, open circles: photoproduction data, full circles: DIS data with $10 < Q^2 < 100$ GeV^2 for $0.3 < y < 0.5$. (b) η^*_{max} distribution per unit of η^* normalized to the total number of events.

photon induced reactions and hadron induced reactions behave very alike in some aspects, independent of the photon virtuality.

Resolved Component of the Photon: Partonic structure of the photon is expected to be suppressed as the virtuality increases[40]. The ZEUS experiment observed the resolved behavior of the photon[41] at a Q^2 known by tagging the scattered electrons,[7] in the Q^2 regions of $10^{-6} < Q^2 < 0.02$ GeV^2, and $0.3 < Q^2 < 0.6$ GeV^2. The x_γ distributions of these events are shown in Fig.14 (a) and (b). The low x_γ, indicative of resolved photons, is clearly observed at Q^2 as high as $0.3 - 0.5$ GeV^2.
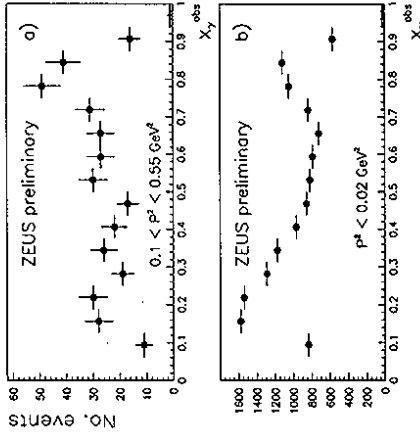
Figure 14: x_γ distribution from events with the scattered electron tagged in the (a) beam pipe calorimeter, and in the (b) electron calorimeter of the luminosity monitor.

Photon structure, gluon content: The quark structure of the photon has been measured in $e\gamma$ interactions by the e^+e^- experiments[42] in the fractional momentum range $0.007 \le x \le 1$. Photoproduction of jets at high energies offers a new tool for determination of the gluon density in the photon in γp interactions at HERA. (Recent high energy e^+e^- experiments are also sensitive to the jets from $\gamma\gamma^*$ interactions[43]). The H1 experiment used hard photoproduction dijet events, with each jet having a minimum transverse momentum, $p_t > 7$ GeV, to define the event sample to extract the photon structure function[44]. Figure 15 (a) shows the x_γ distribution of these events as measured from the jets. The direct photon events are seen at $x_\gamma \sim 1$, where the photon behaves as a point-like object. Using the quark-density photon structure function measured in e^+e^- experiments as input, a fraction of events shown by the solid curve in Fig 15 (a) can be explained. The rest of the events in the spectrum, at lower x_γ, likely indicate the presence of gluons in the photon. The GRV structure function[8]

[7]the electron calorimeter of the luminosity monitor and the Beam Pipe Calorimeter (BPC) detects scattered electrons with $10^{-6} < Q^2 < 0.02$ GeV^2 and $0.3 < Q^2 < 0.6$ GeV^2, respectively.

[8]The Gluck-Reya-Vogt (GRV) structure function of the photon in LO[45], starts with an input parton density at $Q^2 = 0.03$ GeV^2 and then is evolved according to the GDLAP prescription[46].

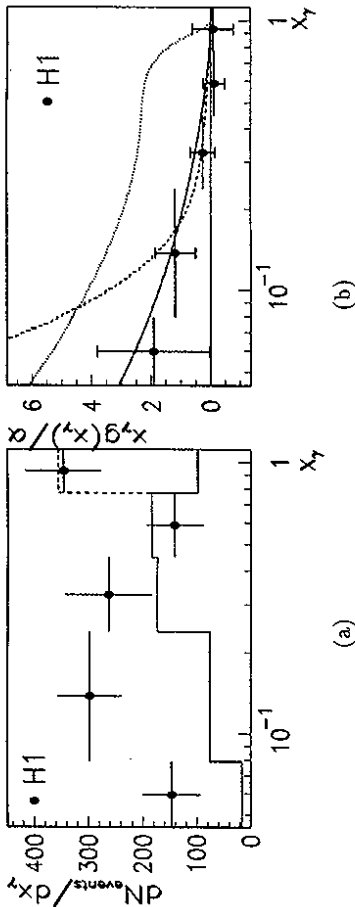of the photon explains the events well, as shown in Fig.15 (b). Input use of

Figure 15: (a) x_γ distribution of the two-jet events. Only statistical errors are displayed. The full line shows the contribution from the quark resolved photon process; the dashed line shows the direct photon contribution as obtained from PYTHIA. (b) The gluon density of the photon divided by the fine structure constant ($\alpha = 1/137$) at $< p_t >^2 = 75$ GeV². For comparison the GRV-LO (full), the LAC1 (dashed), and the LAC3 (dotted) parametrizations of the photon's gluon density are shown.

several other structure functions, LAC1 and LAC3[47], are also shown in the same figure; they do not describe the data so well. The probability of the observed event distribution to be compatible with no gluonic component in the photon is 0.1%. The gluonic component at low x_γ appears to rise faster than the quark content of the photon.

2.7 The Transition Region: The Soft and the Hard Pomeron

The F_2 measurements from DIS can be turned into a γ^*p total cross section by the realation, $\sigma(\gamma^*p) = \frac{4\pi^2\alpha}{Q^2}F_2(W^2_{\gamma p}, Q^2)$ measurements, similar to the way the electroproduction cross sections in Fig. 9 were turned into the γ^*p cross section. Figure 16 is a compilation of the $W_{\gamma p}$ dependence for all the γ^*p cross sections obtained from photoproduction and DIS. At low $Q^2(\simeq 0)$ the cross section decreases with an increase in $W_{\gamma p}$ to a minimum after which there is a slow rise with $W_{\gamma p}$. This was explained earlier as being consistent with soft pomeron (and meson) exchange. As Q^2 increases, the $\sigma(\gamma^*p)$ shows a slow rise followed by a fast rise with increasing $W_{\gamma p}$. The faster rise, thought to be a general consequence of QCD, was described earlier as a signature of hard pomeron exchange. This trend is observed throughout Fig. 16, with the transition from soft to hard pomeron exchange taking place at increasingly lower $W_{\gamma p}$ as Q^2 increases. It is from this region that we hope to gain an understanding of the transition phenomena from non perturbative to perturbative QCD. In photoproduction, this region is approached starting with quasi-real photons and then going towards the transition region. In DIS the approach is to go as low as possible in Q^2 and

x. This will be discussed by the next speaker in detail. At the lowest Q^2 value of 2 GeV², the $\sigma(\gamma^*p)$ in Fig.16 still shows a fast rise.
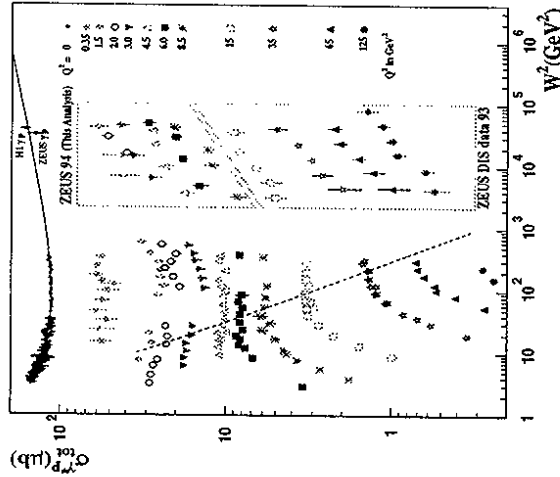

Figure 16: Compilation of total cross sections as a function of $W_{\gamma p}$ at various Q^2 from photoproduction and DIS.

3 The Rapidity Gap Events

The Neutral Current (NC) DIS events are characterized by the detected scattered electron, the current jet caused by the hadronization of the struck quark, and the debris of the remains of the proton (called the proton remnant jet) around the forward beam pipe. As the struck quark leaves the proton, color strings are stretched between the struck quark and the remaining part of the proton: these eventually break up and form hadrons, which in turn deposit energies in the calorimeter between the current jet and the proton remnant. Hence, in a typical NC DIS event, the observed particle with the highest pseudorapidity (η_{max}) and a minimum of (e.g.) 400 MeV energy deposit in the calorimeter has η_{max} above 3 or 4 as shown in Fig.17 (a). In the 1992 NC events sample, a category of events ($\sim 10\%$) were observed with $\eta_{max} \lesssim 2.5$, i.e., as if the proton after the reaction went down the forward beam pipe unchanged. A special class of these events would be exclusive vector meson production in DIS. In QCD terminology a color singlet exchange (e.g. gluon ladder) between the lepton and the proton could explain these events; in Regge terminology these events would represent a hard pomeron exchange.

First observed by ZEUS, both experiments have now seen these events with Large Rapidity Gaps[53] (LRG), characteristic of a pomeron exchange.

Figure 17 (b) shows a diagram of this mechanism for such LRG events. Kinematics of these events are very like the NC DIS events; this will be discussed in detail by the next speaker.
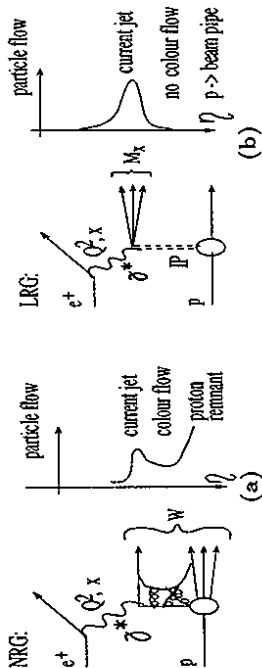
Figure 17: (a) Schematics of ordinary DIS process, without any rapidity gap. (b) Schematics of events with a large rapidity gap.

3.1 Structure Function of the Pomeron

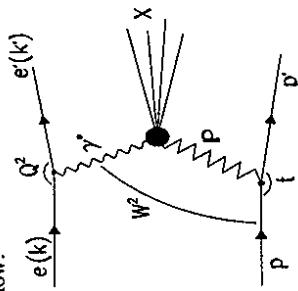The kinematics of a pomeron exchange, are shown in Fig. 18 and are explained below.

Figure 18: Kinematics of an event with a pomeron exchange.

$t = P - P' \simeq 0$

$x_P = \frac{(P-P')\cdot q}{P\cdot q} \simeq \frac{M_X^2 + Q^2}{W^2 + Q^2}$ = momentum fraction of the P in prton

$\beta = \frac{x}{x_P} \simeq \frac{Q^2}{M_X^2 + Q^2} \simeq x_{q/P}$ = momentum fraction of the struck quark in the P

A structure function for the pomeron P from the LRG events in DIS data sample can be defined from:

$$\frac{d^3\sigma}{dx_P dx dQ^2} = \frac{4\pi\alpha^2}{Q^4 x}(1 - y - y^2/2)F_2^{D(3)}(Q^2,\beta,x_P).$$

19

Since the diffracted proton is not observed, $F_2^{D(3)}$ has been integrated over t. If factorization at the pomeron-proton vertex can be assumed, then,

$$F_2^{D(3)}(Q^2,\beta,x_P) = f_{P/p}(x_P)\cdot F_2^{D(2)}(Q^2,\beta),$$

where $f_{P/p}(x_P)$ denotes the pomeron flux. The rapidity gap DIS event samples were divided into bins of Q^2 and β by both H1 and ZEUS experiments. For each data sample, the event distribution as a function of x_P could be fit to a straight line with a slope independent of the Q^2 and the β value. Figure 19 shows the ZEUS[55] and the H1 distributions[54]; a fit to the form
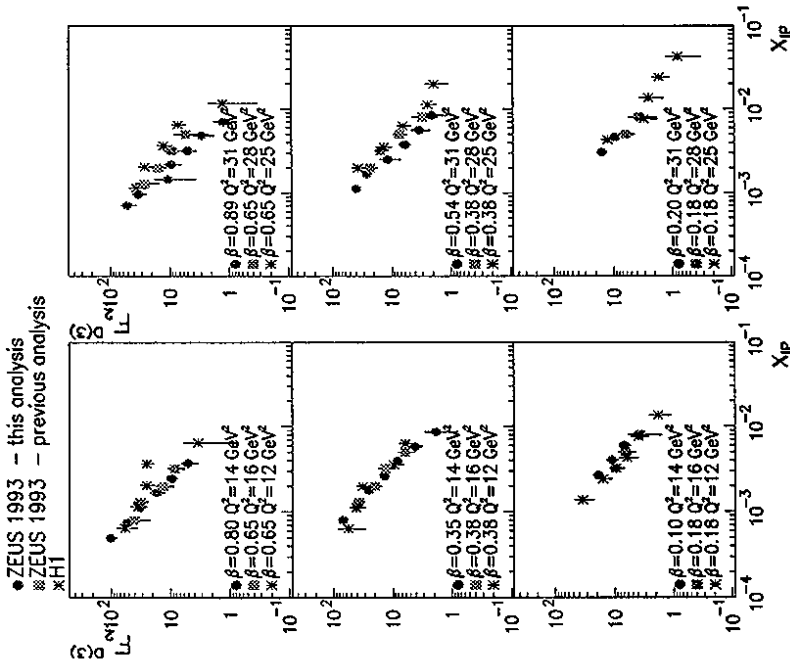
ZEUS 1993 – this analysis
ZEUS 1993 – previous analysis
H1

(a)
β=0.80 Q²=14 GeV²   β=0.89 Q²=31 GeV²
β=0.65 Q²=16 GeV²   β=0.65 Q²=28 GeV²
β=0.65 Q²=12 GeV²   β=0.65 Q²=25 GeV²

β=0.35 Q²=14 GeV²   β=0.54 Q²=31 GeV²
β=0.38 Q²=16 GeV²   β=0.38 Q²=28 GeV²
β=0.38 Q²=12 GeV²   β=0.38 Q²=25 GeV²

β=0.10 Q²=14 GeV²   β=0.20 Q²=31 GeV²
β=0.18 Q²=16 GeV²   β=0.18 Q²=28 GeV²
β=0.18 Q²=12 GeV²   β=0.18 Q²=25 GeV²

Figure 19: $F_2^{D(3)}$ vs x_P for various β values are shown from the H1 data and two different analyses with two selection criteria from ZEUS data.

$b(1/x_P)^a$ (with b varying from bin to bin) yielded $a = 1.19 \pm 0.06 \pm 0.07$ for H1 data and $a = 1.30 \pm 0.08^{+0.08}_{-0.14}$ from the ZEUS data. Hence the data do not violate the factorization assumption. A second more recent analysis from ZEUS is also shown in Fig. 19. The event selection and analysis criteria were entirely different, and will not be described here[56]. The results were consistent with the first analysis; subtracting the non-diffractive background in a way similar to the first analysis[55] gave $a = 1.28 \pm 0.04$, while using a

20

a new method gave $a = 1.42 \pm 0.08$. The uncertainties quoted in the second method are statistical only.

Since the data were consistent with factorization in the available kinematic region, we obtain $F_2^{D(2)}$ by integrating over the observed kinematic x_P range. The $F_2^{D(3)}$ distributions vs β and Q^2 for H1 and ZEUS data and the $F_2^{D(3)}$ vs β for ZEUS data are shown in Fig. 20. A soft momentum distribution of the pomeron constituents like $(1-\beta)^n$, where n is a positive integer does not fit the data shown; a harder distribution like $\beta(1-\beta)$ is preferred. Both are superimposed on the ZEUS data. The data seem to prefer a combination of hard with a slight mixture of soft distribution.
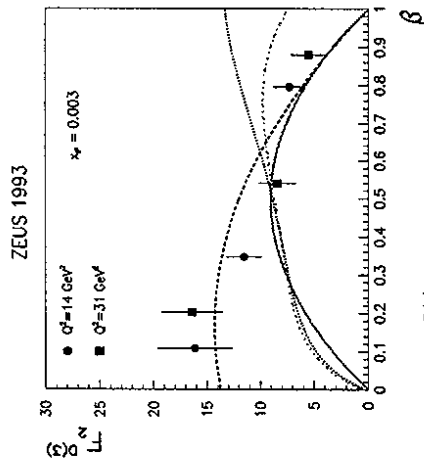

Figure 20: $F_2^{D(3)}$ vs β obtained from the ZEUS analyses.

Contents of the Pomeron: In DIS the highly virtual photon couples to quarks in lowest order. But, in hard photoproduction when jets are observed, both quarks and gluons in the proton can couple to the virtual photon in the lowest non-vanishing order. The LRG events have also been observed in photoproduction events[57]. So, by comparing the rapidity gap events of DIS and hard photoproduction, ZEUS has estimated the relative gluon content of the pomeron inside the proton. Events with jets having $E_t \geq 8$ GeV in the central region ($-1 \leq \eta \leq 1$) were selected. Similar to the DIS LRG events, the distribution of the photoproduction LRG events prefered a hard partonic component in the $\mathcal{P}$. Assuming all of the pomeron momenta are carried by its partonic contents, i.e., using the momentum sum rule $\int d\beta \Sigma_i \beta f_{\mathcal{P}/p}(\beta) = 1$, the event distribution in terms of η_{max} of the events favors hard gluon content. The non-diffractive contribution was modeled by the MC and a double-diffractive contribution of $\sim 15\%$[55] where the proton diffractively dissociated, was subtracted.

As the momentum sum rule need not apply to the constituents of the $\mathcal{P}$, this was not imposed to the data for further analysis. The total momentum carried by the pomeron was then measured as a function of C_g, the relative ratio of gluonic to quark content of the pomeron without the momentum sum rule restriction. This was performed for both the photoproduction

and the DIS jet sample by the ZEUS collaboration[58]. Figure 21 shows the result with 1σ uncertainty for both. The two curves intersect around
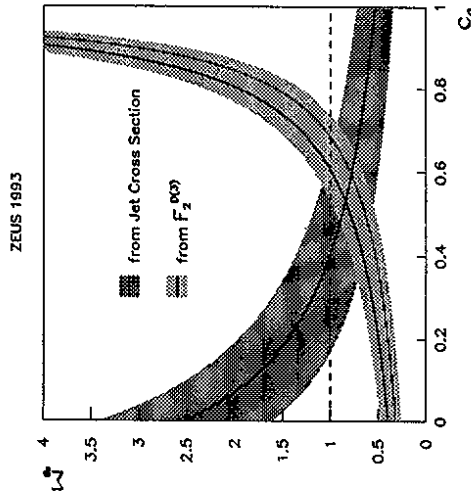

Figure 21: The total momentum of the pomeron as a function of the ratio of its gluon partonic content and quark partonic content from the LRG events from the DIS event sample and the hard photoproduction event sample. The intersection of the two samples yield a ratio of $\sim 2 : 1$ gluon to quark partonic content of the pomeron without the need for any momentum sum rule for the partons from the pomeron.

$C_g = 0.6$, i.e., both set of data are satisfied with a relative gluonic component of 0.6 and a quark content of 0.4 in the pomeron without the need for the momentum sum rule. The assumption made is that same $\mathcal{P}$ is observed in both photoproduction and DIS; the momentum sum rule has not been applied. It should be noted that the total momentum in the DIS sample rises very steeply as C_g approaches 1, reflective of the fact that the lowest order coupling of the virtual photon in DIS to the proton is to its valence quarks.

4 Conclusion and Future Plans

The ep colliding beam experiments, H1 and ZEUS, have made remarkable progress towards understanding the transition betweeen the regions where non-perturbative and perturbative QCD apply. For quasi-real photons, low p_t, and light quark vector mesons, the elastic photoproduction follows the VDM-Regge non-perturbative prediction. However, as we get to heavy quarks e.g., photoproduction of J/ψ, or to high virtuality, e.g., exclusive production of light quark vector mesons in DIS, or photoproduction at high transverse momenta, some pQCD calculations begin to be applicable. In any case, the non-perturbative predictions do not apply as observed from the steeper rise of cross section of photoproduction of J/ψ with in-

creasing $W_{\gamma p}$ than predicted by DL[17] calculations. The DIS exclusive production of J/ψ does not hold any surprise since the pQCD scale has already been set. The diffractive scattering or pomeron exchange at an appropriate scale can then be described in terms of pQCD. The changing nature of pomeron is being studied extensively. The study of the structure function of pomeron in DIS has started, many new results are forthcoming in this area. A large amount of literature is available on the diffractive interactions[59, 12, 60, 9, 61, 62, 63]. We have also studied the pomeron contents, and observed substantial presence of gluonic partons. The structure of photons have revealed new information, that at low x the gluonic content of the photon increases. And, presence of partonic structure in the photon can be observed at a Q^2 as high as $0.3 - 0.6$ GeV^2.

Upgrades to cover more phase space with better resolution have been added in 1995. The H1 experiment has recently added a silicon vertex detector and a silicon rear detector. The ZEUS group completed all six stations of LPS which helps detect the intact outgoing proton. The Beam Pipe Calorimeter has been replaced with a W-scintillator sampling calorimeter with a larger coverage of $0.1 \leq Q^2 \leq 0.8$ GeV^2. In addition, a scattered electron tagger 44 m away from the IP in the rear direction at $80 < W_{\gamma p} < 100$ GeV, a proton remnant taggers around the forward direction, and a presampler to the F and R calorimeter (to understand the energy scale), have also been installed. The early look at the 1995 data indicates the technical as well as physics success of these upgrades. The 1994 data at HERA provided a unique kinematic domain to understand QCD, to study photon, pomeron and proton structures. With the 1995 upgrades, both H1 ans ZEUS detectors are well on their way to provide the best understanding of these topics. (Many interesting topics, like strange quark studies and different approaches for understanding color singlet exchange in both H1 and ZEUS experiments, are not covered due to lack of time and space.)

References

[1] M. Riordan, The Hunting of Quark, Simon & Schuster, New York; R. Taylor, Proceedings of the 19th SLAC Summer Institute on Particle Physics, ed. by J.Hawthorne, SLAC-REP-398, 1991 and references therein.

[2] J.T. Friedman and H.W. Kendall, Ann. Rev. Nucl. Sci. 22 (1972) 203.

[3] For a review, see, T. Sloan, G. Smadja and V. Ross, Phys. Rep. 130 (1988) 45; E665 Collab. M.R. Adams et al., Phys. Rev. D 48 (1993) 5057.

[4] For a review, see, S.R. Mishra and F. Sciulli, Ann. Rev. Nucl. Part. Sci. 39 (1989) 259.

[5] H1 Collab., T. Ahmed et al., The H1 Detector at HERA, DESY 93-103.

[6] ZEUS Collab., The ZEUS Detector, Status Report 1993, DESY 1993; ZEUS Collab., M. Derrick et al., Phys. Lett. B 293 (1992) 465.

[7] J.J. Sakurai, Phys. Rev. Lett. 22 (1969) 981.

[8] For a review, see, D.W.G.S. Leith, High Energy Photoproduction: Diffractive Processes, SLAC-Pub-1878, 'Electromagnetic Interaction of Hadrons', Edited by A. Donnachie & G. Shaw, Plenum Publ. Co.;

[9] K. Goulianos, Phys. Rep. 101 (1983) 169.

[10] C.F.von Weizsäcker, Z. Phys. 88 (1934) 612; E.J. Williams, Phys. Rev. 45 (1934) 729.

[11] D.O. Caldwell et al., Phys. Rev. Lett. 40 (1978) 1222.

[12] A. Donnachie and P.V. Landshoff, Nucl. Phys. B 244 (1984) 322; A. Donnachie and P.V. Landshoff, Phys. Lett. B 185 (1987) 403; A. Donnachie and P.V. Landshoff, Nucl. Phys. B 311 (1989) 509; P.V. Landshoff, Nucl. Phys. B(Proc. Suppl.) 18C (1990) 211.

[13] CDF Collab. Phys. Rev. D 50 (1994) 5535.

[14] A. Donnachie and P.V. Landshoff, Phys. Lett. B 296 (1992) 227.

[15] H. Abramovich, E.M. Levin, A. Levy and U. Maor, Phys. Lett. B 269 (1991) 465.

[16] G.A. Schuler and T. Sjöstrand, Phys. Lett. B 300 (1993) 169; G.A. Schuler and T. Sjöstrand, Nucl. Phys. B 407 (1993) 539.

[17] A. Donnachie and P.V. Landshoff, Phys. Lett. B 348 (1995) 213.

[18] ZEUS Collab., M. Derrick et al., Z. Phys. C 69 (1995) 39.

[19] H1 Collab., S. Aid et al., DESY-95-251, to appear in Nucl. Phys. B.

[20] ZEUS Collab., M. Derrick et al., DESY-96-067, to appear in Phys. Lett. B.

[21] ZEUS Collab., The ZEUS Detector, Status Report 1993.

[22] E401 Collab, M. Binkley et al., Phys. Rev. Lett. 48 (1982) 73; E516 Collab., B.H. Denby et al., Phys. Rev. Lett. 52 (1984) 795.

[23] M. Ryskin, Z. Phys. C 57 (1993) 89.

[24] J. Nemchik, N.N. Nikolaev and B.G. Zakharov, Phys. Lett. B341 (1994) 228.

[25] ZEUS Collab., M. Derrick et al., Phys. Lett. B 350 (1995) 120.

[26] H1 Collab., S. Aid et al., DESY-96-037, to appear in Nucl. Phys. B.

[27] H. Jung et al., Z. Phys C 60 (1993) 721; M. Kramer et al., Phys. Lett. B348 (1995) 677; M. Kramer, Nucl. Phys. B459 (1996) 3.

[28] R.K. Ellis and P. Nason, Nucl. Phys. B312 (1989) 551; P. Nason, S. Dawson and R.K. Ellis, Nucl. Phys. B303 (1988) 607; J. Smith and W.L.van Neerven, Nucl. Phys. B374 (1992) 36.

[29] ZEUS Collab., M. Derrick et al., Phys. Lett. B349 (1995) 225.

[30] S.J. Brodsky et al., Phys. Rev. D50 (1994) 3134.

[31] I.F. Ginzburg et al., TPI-MINN-94-14-T, submitted to Nucl. Phys. B.

[32] ZEUS Collab., M. Derrick et al., Phys. Lett. B 356 (1995) 601.

[33] H1 Collab., S. Aid et al., DESY-96-023, to appear in Nucl. Phys. B.

[34] ZEUS Collab., M. Derrick et al., DESY-96-067, to appear in Phys. Lett. B.

[35] ZEUS Collab., M. Derrick et al., Phys. Lett. B 348 (1995) 665.

[36] ZEUS Collab., M. Derrick et al., DESY-96-094, to appear in Phys. Lett. B.

[37] L.E. Gordon and J.K. Storrow, Z. Phys. C 56 (1992) 307.

[38] K. Schilling et al., Nucl. Phys. B 15 (1970) 397; K. Schilling and G. Wolf, Nucl. Phys. B 61 (1973) 381; P. Joos et al., Nucl. Phys. B 113 (1976) 53.

[39] H1 Collab., S. Aid et al., Phys. Lett. B358 (1995) 412.

[40] M. Drees and R. Godbole, hep-ph/9508221.

[41] ZEUS Collab., M. Derrick et al., Phys. Lett. B 354 (1995) 163.

[42] Ch. Berger and W. Wagner, Phys. Rep. 146 (1987) 1 and references therein.

[43] AMY Collab., B.J. Kim et al., Phys. Lett. B325 (1994) 248; TOPAZ Collab., H. Hayashi et al., Phys. Lett. B314 (1993) 149; ALEPH Collab., D. Buskulic et al., Phys. Lett. B313 (1993) 509; DELPHI Collab., P. Abreu et al., Phys. Lett. B342 (1995) 320.

[44] H1 Collab., T. Ahmed et al., Nucl. Phys. B445 (1995) 195.

[45] M. Glück, E. Reya and A. Vogt, Phys. Rev. D46 (1992) 1973.

[46] V.N. Gribov and L.N. Lipatov, Sov. J. Nucl. Phys. 15 (1972) 438 and 675; G. Altarelli and G. Parisi, Nucl. Phys. B 126 (1977) 298; Yu.L. Dokshitzer, Sov. Phys. JETP 46 (1971) 641.

[47] H. Abramowicz, K. Charchula and A. Levy, Phys. Lett. B269 (1991) 458.

[48] A.D. Martin, W.J. Stirling, Phys. Lett. B354 (1995) 155.

[49] Various parameterizations by CTEQ Collab., see e.g., J. Botts et al., Phys. Lett. B 304 (1993) 159 etc.

[50] M. Glück, E. Reya and A. Vogt, Z. Phys. C67 (1995) 433.

[51] H1 Collab., I. Abt et al., Phys. Lett. B321 (1994) 161; M. Roco, PhD Thesis, Univ. of Iowa, DESY Int. Rep. F35D-94-04.

[52] ZEUS Collab., M. Derrick et al., Phys. Lett. B345 (1995) 576.

[53] ZEUS Collab., M. Derrick et al., Phys. Lett. B315 (1993)481; ZEUS Collab., M. Derrick et al., Phys. Lett. B332 (1994)228; H1 Collab., T. Ahmed et al., Nucl. Phys. B429 (1994) 477.

[54] H1 Collab., T. Ahmed et al., Phys. Lett. B348 (1995) 681.

[55] ZEUS Collab., M. Derrick et al., Z. Phys. C68 (1995) 569.

[56] ZEUS Collab., M. Derrick et al., DESY-96-018, to appear in Z. Phys. C.

[57] ZEUS Collab., M. Derrick et al., Phys. Lett. B 346 (1995) 399; H1 Collab., T. Ahmed et al., Nucl. Phys. B 435 (1995) 3.

[58] ZEUS Collab., M. Derrick et al., Phys. Lett. B 356 (1995) 129.

[59] P.D.B. Collins, An Introduction to Regge Theory and High Energy Physics, Cambridge University Press, Cambridge, 1977.

[60] G. Ingelman and P. Schlein, Phys. Lett. B 152 (1985) 256.

[61] L.N. Lipatov, Sov. J. Nucl. Phys. 23 (1976) 338; E.A. Kuraev, L.N. Lipatov and V.S. Fadin, Sov. Phys. JETP 45 (1977) 199; Y.Y. Balitsky and L.N. Lipatov, Sov. J. Nucl. Phys. 28 (1978) 822.

[62] N.N. Nikolaev and B.G. Zakharov, Z. Phys. C 53 (1992) 331.

[63] A. Capella et al., Phys. Lett. B 343 (1995) 403.